HHS Public Access

Author manuscript

Cell Rep. Author manuscript; available in PMC 2020 February 11.

Published in final edited form as:

Cell Rep. 2020 January 28; 30(4): 959–968.e3. doi:10.1016/j.celrep.2019.12.084.

Circuit Integration Initiation of New Hippocampal Neurons in the Adult Brain

Chih-Hao Yang[1,5,6], **Adrian Di Antonio**[2,6], **Gregory W. Kirschen**[3,6], **Parul Varma**[4], **Jenny Hsieh**[4], **Shaoyu Ge**[5,7,*]

[1]Department of Pharmacology, School of Medicine, College of Medicine, Taipei Medical University, Taiwan

[2]Program in Neuroscience, SUNY at Stony Brook, Stony Brook, NY 11794, USA

[3]Medical Science Training Program, Renaissance School of Medicine at Stony Brook University, Stony Brook, NY 11794, USA

[4]Department of Biology and Brain Health Consortium, The University of Texas at San Antonio, San Antonio, TX 78249, USA

[5]Department of Neurobiology & Behavior, SUNY at Stony Brook, Stony Brook, NY 11794, USA

[6]These authors contributed equally

[7]Lead Contact

SUMMARY

In the adult brain, new dentate granule cells integrate into neural circuits and participate in hippocampal functioning. However, when and how they initiate this integration remain poorly understood. Using retroviral and live-imaging methods, we find that new neurons undergo neurite remodeling for competitive horizontal-to-radial repositioning in the dentate gyrus prior to circuit integration. Gene expression profiling, lipidomics analysis, and molecular interrogation of new neurons during this period reveal a rapid activation of sphingolipid signaling mediated by sphingosine-1-phosphate receptor 1. Genetic manipulation of this G protein-coupled receptor reveals its requirement for successful repositioning of new neurons. This receptor is also activated by hippocampus-engaged behaviors, which enhances repositioning efficiency. These findings reveal that activity-dependent sphingolipid signaling regulates cellular repositioning of new dentate granule cells. The competitive horizontal-to-radial repositioning of new neurons may provide a gating strategy in the adult brain to limit the integration of new neurons into pre-existing circuits.

*Correspondence: shaoyu.ge@stonybrook.edu.

AUTHOR CONTRIBUTIONS

C.-H.Y. and S.G. conceived the project. C.-H.Y., A.D.A., and G.W.K. performed experiments and analyzed data. P.V. and J.H. provided RNA-seq data and analysis. C.-H.Y., A.D.A., and G.W.K. wrote the initial draft of the manuscript. All authors edited the manuscript and approved the final version.

SUPPLEMENTAL INFORMATION

Supplemental Information can be found online at https://doi.org/10.1016/j.celrep.2019.12.084.

DECLARATION OF INTERESTS

The authors declare no competing interests.

Graphical Abstract

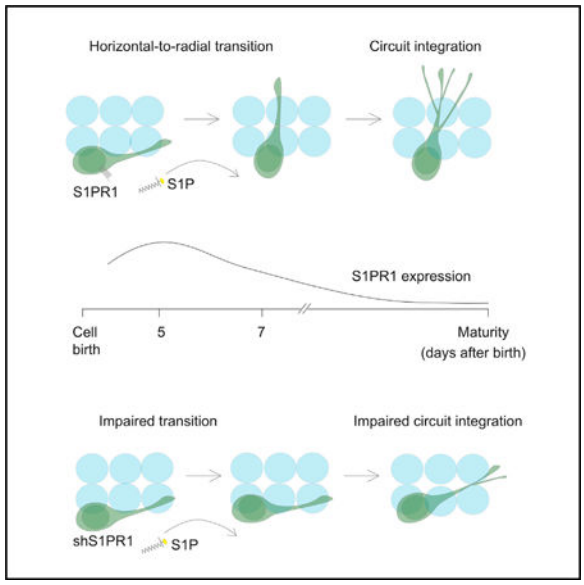

In Brief

Yang et al. show that prior to circuit integration, adult-born dentate granule cells undergo horizontal-to-radial transitioning, which is regulated by sphingolipid signaling via sphingosine-1phosphate receptor 1.

INTRODUCTION

The subgranular zone of the adult hippocampus continuously gives rise to new dentate granule cells (DGCs) (Altman and Das, 1965; Christian et al., 2014; Eriksson et al., 1998; Kempermann et al., 1997). A proportion of these survive an initial developmental phase, termed the “critical survival period,” and functionally integrate into the pre-existing hippocampal circuit (Espósito et al., 2005; Ge et al., 2006; Gonçalves et al., 2016; Gu et al., 2012; Overstreet Wadiche et al., 2005; Sahay et al., 2011; Song et al., 2013; Tashiro et al., 2006; van Praag et al., 2002). The survival of these cells during their first 2 weeks is enhanced by hippocampus-engaged environmental exploration (EE) (Kempermann et al., 1997; Kirschen et al., 2017).

Recent studies from our laboratory and others using either retroviral or transgenic labeling showed that newly generated DGCs are positioned similar to existing DGCs and form stable functional synapses as early as 14 days after birth (Espósito et al., 2005; Ge et al., 2006; Overstreet Wadiche et al., 2005). Morphological analyses revealed that most of these newly generated DGCs were initially positioned horizontally, parallel to the DGC layer (Sun et al., 2015). Thus, since mature DGCs are oriented radially, the newly generated DGCs must transition from a horizontal to a radial orientation during early phases of integration. However, the mechanism for this repositioning and the influence this has on the survival and initial integration of DGCs into the circuit remain poorly understood.

In this study, we used live imaging to birthdate (i.e., determine date of birth) and monitor the development of newly generated retrovirally labeled DGCs. A competitive horizontal-to-radial repositioning of newly generated DGCs occurs involving dynamic neurite remodeling prior to functional synapse formation. Hippocampus-engaged activities affect the efficiency of repositioning, and these processes involve metabolically regulated sphingolipid signaling critical for integration.

RESULTS

Circuit Integration Initiation of Newly Generated DGCs Starts with Horizontal-to-Radial Repositioning

To investigate the development of newly generated DGCs prior to functional circuit formation in the adult brain, we infected newborn DGCs in mice with a retrovirus to express green fluorescent protein (GFP). These cells became post-mitotic around 4 days postinfection (dpi), at which time the mitotic marker minichromosomal maintenance (MCM) is turned off (Wang et al., 2019). Consistent with previous work (Sun et al., 2015), most GFP $^{+}$ cells were positioned horizontally (parallel to the DGC layer) at 5 dpi, whereas none were horizontal at 14 dpi (Figure 1A). Accordingly, the angles of the cellular axis of orientation (relative to the DGC layer) of most GFP^{+} cells at 5 dpi were between 15°and 20°, whereas all GFP^{+} cells were at angles between 30°and 90°at 14 dpi, similar to mature DGCs (Figure 1B). At 7 dpi, the angles for only a small proportion of the GFP^{+} cells were similar to those of 5 dpi cells, suggesting that horizontal-to-radial cellular repositioning occurred between 5 and 7 dpi. Given that the transition from 5 to 7 days appeared to be centered on a shift from less than 20 to greater than or equal to 20, we defined 20 as the threshold delineating the horizontal versus radial dichotomy.

The horizontally positioned GFP^{+} cells at 5 dpi expressed both prospero homeobox protein 1 (Prox1; DGC marker) and doublecortin (DCX) (Figure 1C, left), suggesting immature DGC identity. This was further validated by the presence of Na^{+} currents (as neuronal fate is sealed, a depolarizing component of the action potential representing the Na^{+} current appears; He et al., 2015) recorded from 5/7 horizontally positioned GFP^{+} cells at 5 dpi, as well as other electrophysiological parameters (Figure 1C, right; Table S1). None of the horizontally positioned DGCs at 5 dpi responded to stimulation of local dentate gyrus (DG) neural circuits (Ge et al., 2006), indicating a lack of functional synapses. By contrast, 4/11 radially positioned GFP^{+} cells showed synaptic GABAergic responses with an amplitude of ~3 pA at 7 dpi (Table S2), consistent with our previous observation (Ge et al., 2006). Morphological measurements of the neurites of horizontally positioned DGCs revealed similar numbers of branches and total process lengths at 5 and 7 dpi, with expansion from 14 dpi to 56 dpi (Figures 1D and 1E), suggesting minimal structural remodeling during this initial phase that occurs substantially soon after repositioning (Ge et al., 2006).

At 4 dpi, newly generated DGCs were live imaged every 30 min in culture for 2 days with a high-throughput live imaging system comprising a spinning disk confocal microscope and incubator (Figure 1F). We imaged using a large field of view (200 × 200 μm) to guard against the possibility that cells might have migrated away during the imaging period. Most GFP^{+} DGCs were horizontally positioned relative to the DGC layer in the neurogenic zone.

As shown in Figure 1G and Video S1, these GFP^+ DGCs dynamically extended and retracted processes in the neurogenic zone, with a bias toward the DGC layer. During the 2-day imaging period, ~56% (30/54) of these cells formed neurites from the leading expansion that rapidly extended into the DGC layer before establishing a radial orientation. This leading process may develop into the apical dendrite (Rao et al., 2018) and thus was termed the primary neurite. The remaining 24 cells ceased to grow, and most disappeared from the field of view during the imaging period (Figure 1H), suggesting the death of these cells. Further analyses revealed that very few of the repositioned cells were successful on the first attempt, with most requiring two or three tries involving reformation of the leading process in different locations before successfully transitioning to a radial orientation (Figure 1I). Once repositioned, these new DGCs with apical neurites radially migrate into the DGC layer (Video S2) for synaptic integration (Ge et al., 2006). We tracked 14 cells after repositioning for another 5 days, among which only two ceased to grow and disappeared, suggesting successful repositioning may be essential for new DGCs to survive.

Thus, horizontally positioned new DGCs extend newly formed neurites into the DGC layer to reposition from a horizontal to a radial orientation between 5 and 7 dpi, before circuit integration. That these cells extend multiple primary neurites suggests the cells might compete for the best location for repositioning, and those that do not reposition are eliminated.

S1PR1 Is Activated in Newly Generated DGCs Prior to Repositioning

To begin to explore the cellular mechanisms underlying the horizontal-to-radial repositioning of newly generated DGCs, we performed RNA sequencing (RNA-seq) analysis of cultured adult hippocampal neural stem cells (NSCs) at 1 day after neuronal differentiation. Neuronal stem cell cultures were derived from NSCs, and cultures were treated with retinoic acid and forskolin to achieve neuronal differentiation, as described in the STAR Methods. Given that active cell growth and neurite remodeling likely have high metabolic demands (Figures 1F–1H), we focused on changes in metabolic-signaling-related genes. We identified pronounced changes in sphingolipid-signaling-related gene expression. Among these, there was a prominent increase in the expression of the sphingosine-1-phosphate receptor 1 (S1PR1) (Figure 2A), shown to be involved in cellular growth in many cell lines, as well as of sphingosine kinase 1 (SPHK1), the enzyme that phosphorylates sphingosine into the active ligand sphingosine-1-phosphate (S1P) (Hannun and Obeid, 2008). Based on this suggestive screen, we chose to investigate the possible role of S1PR1 on the horizontal-to-radial repositioning of new DGCs, given that this cell-membrane-bound receptor may be more directly implicated in the cells' sensing of their local microenvironment, which may help orient them for proper positioning in order to establish circuit integration.

Since metabolic demands of *in vitro* cultures differ from those in vivo, we looked at the gene expression profiles of 14-day-old GFP-labeled immature neurons in wild-type (WT), pilocarpineinduced seizures, and chemo-genetically silenced (DREADD) conditions (unpublished data). It has been shown that seizures accelerate the functional integration of newborn neurons and also lead to the production of ectopic granule cells (Overstreet

Wadiche et al., 2006; Scharfman et al., 2007). Therefore, if sphingolipid molecules are involved in the proper maturation and repositioning of newborn neurons under physiological conditions, dysregulation of the same pathways should occur in pathological conditions such as seizures. We find that S1PR1 is downregulated with seizures and seems to be restored (upregulated) with silencing of the immature neurons after pilocarpineinduced seizures. These lines of evidence from both in vitro and in vivo studies led us to investigate a possible role of S1PR1 in the neurite remodeling of newly generated DGCs.

We first confirmed that S1PR1 mRNA is expressed in the DG (Figure 2B). We then immunostained hippocampal sections for the protein and observed a particularly strong signal in the inner DG cell layer, where the neurogenic niche is located. S1PR1 immunoreactivity was present on virtually all DCX^+ neurons, including the horizontally positioned ones (Figure 2C). The S1PR1 expression on new DGCs was further confirmed using retrovirus-labeled cells at 7 dpi (Figure 2D). S1PR1 expression peaked at 5 dpi, decreased by 7 dpi, and was minimally expressed by 56 dpi (Figure S1). Consistent with a potential role of S1PR1 in facilitating the horizontal-to-radial transition, we observed lower levels of S1PR1 in radial cells, compared to horizontal cells at the same developmental age of 7 dpi (Figure S2).

As S1PR1 is activated by an endogenous biologically active metabolite ligand S1P (Hannun and Obeid, 2008), we performed a lipidomics analysis to measure sphingolipid metabolites in acutely dissected hippocampal subfields, as well as in neocortex for comparison (Figure 2E). A complete set of lipid metabolites in the S1P synthesis pathway was detected in these tissues (Figure 2F). We noted a significant difference in lipid profiles between the DG and the neocortex (used as a control region) (Figure 2F). We then confirmed pathway activation in the DG by immunostaining for the activated form of the receptor, which is phosphorylated on residue Thr236 (Lee et al., 2001). We found that approximately 36% of DCX^+ cells (31/85) were activated under basal conditions (Figure 2G); ~55% (17/31) of these were horizontally positioned DGCs.

Altogether, our results from gene expression profiling, lipidomic, and immunostaining analyses of hippocampal sections reveal that sphingolipid signaling, especially via S1PR1, is promptly activated in newly generated DGCs prior to circuit integration, suggesting a potential role of this pathway in regulating initial development of newly generated DGCs.

S1PR1 Regulates the Horizontal-to-Radial Repositioning of Newly Generated DGCs

To determine whether S1PR1 signaling is required for the horizontal-to-radial repositioning of newly generated DGCs, we infected the cells of the DG with retroviral vectors encoding short-hairpin RNA against S1PR1 (shS1PR1) to knockdown expression or against luciferase (shLuc) as a control (Figure 3A). We designed four shS1PR1 vectors, of which two were found to be highly efficient at knockdown, although viral titers were low, with approximately 10–15 cells labeled per injected mouse. To avoid any confounding effects on the proliferation and differentiation of neural progenitors, we included doxycycline (DOX)-inducible elements in the retroviral vectors as illustrated in Figure 3A or as recently reported (Rao et al., 2018). After viral infusion into the DG, we induced short hairpin RNA (shRNA) expression starting at 3 dpi using 5 mM DOX added to the drinking water (Kumamoto et al.,

2012; Rao et al., 2018). Knockdown of S1PR1 was detectable at 5 dpi in cells infected with shS1PR1, compared to expression in cells infected with shLuc, verified by immunostaining for S1PR1 (Figure 3B). Whereas shLuc$^+$ DGCs underwent a horizontal-to-radial transition from 5 to 7 dpi similar to that observed in Figure 1B, the angle distribution of shS1PR1$^+$ DGCs did not change (Figures 3C and 3D). Note that at 5 dpi, both groups showed similar percentages of horizontally positioned new DGCs, but this percentage declined only in the shLuc$^+$ cells (Figure 3E). Accordingly, the newly generated DGCs with S1PR1 knockdown had fewer neurites at 6 and 7 dpi than did control cells (Figure 3E). In line with these findings, knockdown cells exhibited fewer spontaneous excitatory postsynaptic currents (sEPSCs) at 21 dpi, although the amplitude of these currents was unaffected, suggesting decreased synaptic input onto knockdown cells versus control cells without changes in cell-intrinsic properties (Figure 3F).

To further exclude the possibility that the effects of S1PR1 knockdown resulted from delayed neuronal development, we performed whole-cell recordings at 5 and 7 dpi. The membrane potentials and resistances were similar between the shS1PR1$^+$ and shLuc$^+$ DGCs at 7 dpi (Table S3). Although we did not statistically analyze the number of new DGCs in this set of experiments, we did not observe obvious differences in the numbers of labeled cells at 5 dpi, suggesting that S1PR1 knockdown might not affect their survival.

To examine whether S1PR1 activity is sufficient to promote repositioning, we expressed mouse S1PR1 in newly generated DGCs using a DOX-inducible retroviral vector (Kumamoto et al., 2012; Figure 3G). We administered these injected mice with DOX from 4 dpi to induce the expression of S1PR1 or GFP only (control) in infected newborn DGCs. Overexpression was induced at 4 dpi and substantially decreased the proportion of horizontally positioned DGCs at 6 and 7 dpi (Figures 3H and 3I). Additionally, DGCs overexpressing S1PR1 had more neurites (Figure 3I), implicating neurite remodeling in repositioning. Furthermore, cells overexpressing S1PR1 exhibited more sEPSCs without a change in sEPSC amplitude, suggesting increased synaptic input without changes in cell-intrinsic properties.

Together with the findings from knockdown experiments, these results reveal that S1PR1 is necessary and sufficient for repositioning and neurite growth of newly generated DGCs. S1PR1 expression in newly generated DGCs is likely essential for successful cellular repositioning prior to circuit integration.

Hippocampus-Engaged Enriched EE Promotes the Horizontal-to-Radial Repositioning of Newly Generated DGCs through S1PR1 Activation

Only a portion of newborn DGCs succeed in repositioning prior to circuit integration during the early stage of development. We therefore asked whether hippocampus-engaged behaviors, shown to regulate the survival of newborn DGCs during this critical phase (Kempermann et al., 1997), influence the repositioning efficiency to control the number of new neurons surviving prior to circuit integration.

Hippocampus-engaged EE robustly promotes the survival of newly generated DGCs during the first 2 weeks after birth (Kempermann et al., 1997; Kirschen et al., 2017). The

repositioning of DGCs at 5 to 6 dpi was examined in mice housed in their home cage (HC) or one containing 4 to 6 novel objects (EE) to assess the impact of hippocampal engagement on the efficiency of repositioning (Figure 4A). There were substantially more GFP^+ DGCs with primary neurites extending into the DGC layer in animals housed in EE cages than in HCs (Figure 4B). The proportion of GFP^+ DGCs with primary neurites with angles ranging from 20°to 90°was 2-fold higher in animals housed in EE cages than in the HC group (Figures 4C and 4D). The percentage of radial GFP^+ DGCs increased from 5 dpi to 8 dpi, with radial repositioning of new DGCs in the EE group almost complete by 7 dpi versus 10 dpi in the HC group (Figure S3). These results demonstrate that the repositioning of newly generated DGCs is facilitated by hippocampus-engaged EE, which may be mediated by increased neurite growth.

These latter experiments document the roles of EE and S1PR1 on the repositioning of newly generated DGCs. Thus, we hypothesized that EE may induce S1PR1 activity to regulate DGC development. Indeed, we found that 1 h of hippocampus-engaged exploration enhanced the phosphorylation of the S1PR1 G-protein-coupled receptor in newly generated (DCX^+) DGCs, including horizontally positioned cells, although total levels of S1PR1 did not change (Figure 4E). This activation was shortlived, decaying after several hours (data not shown). To determine whether the elevated phosphorylation of S1PR1 causes increased neurite development, we induced S1PR1 activation *in vitro* to confirm the effects on neurite remodeling in cultured hippocampal neurons. The cells were cultured for 2 days with various doses of S1P ranging from 0 to 100 μM (on the basis of the amounts measured in tissues in the lipidomics analysis, which were calculated for the weight and volume of DG tissue). S1PR1 activation, as assessed by levels of immunoreactivity for the phosphorylated receptor, increased with increasing doses of S1P (Figures S4A and S4B). Application of as little as 1 nM S1P substantially promoted the phosphorylation and neurite arborization, evidenced as increases in the numbers of branch points and total neurite length. All were enhanced further at higher doses of S1P (Figures S4B and S4C). The increase in branching with S1P-induced receptor activation was abrogated in cells expressing shS1PR1 (Figure S4D), confirming that the activation of S1PR1 regulates DGC neurite remodeling and consistent with the effects of EE *in vivo*. Notably, peak activation *in vitro* occurred with 10 nM S1P and was similar to the effect with 100 nM. Previous findings from endothelial cells indicated that a high dose of S1P decreasesS1PR1 activity, possibly due to receptor internalization (Chavez et al., 2015).

To determine whether the repositioning of newly generated DGCs that was enhanced under EE conditions required S1PR1 activation, we induced the expression of retroviral vectors encoding shS1PR1 or shLuc at 3 dpi and then housed the animals in either HC or EE cages at 5 dpi; the orientation of GFP^+ DGCs was then assessed at 6 dpi (Figure 4F). The increase in the proportion of DGCs angled between 20°and 90°was not observed in the cells with S1PR1 knockdown ($shS1PR1^+$) (Figure 4G). Similarly, the increase in neurite number was abrogated by S1PR1 knockdown (Figure 4G). Furthermore, the angle distributions of these cells under both conditions were similar up to 10 dpi (i.e., EE no longer facilitated the radial repositioning of these cells) (Figure 4H). There was no obvious difference in the numbers of horizontally or radially positioned new DGCs (Figure 4H). We should point out that although we found no obvious increase of the repositioning rate in shS1PR1+ cells, the trend

of increased radial angling for these cells in the context of EE remains, suggesting the possible involvement of other regulatory mechanisms. The presence of the trend may also be from incomplete knockdown. These results indicate that S1PR1 activation by hippocampus-engaged exploration regulates neurite remodeling and thus DGC repositioning from horizontal to radial.

Altogether, this line of evidence suggests that as they remodel their neurites, newly generated DGCs undergo an essential developmental stage of repositioning that is experience regulated and partially reliant on sphingolipid signaling. Such experience, in the form of hippocampus-engaged activities, may serve as a gating mechanism to control the success rate of new DGCs competing to initiate circuit integration.

DISCUSSION

Local circuit activity is important for neurite growth, integration, and neurogenesis (Gonçalves et al., 2016). New DGCs begin to form synapses at 1 week of age (Ge et al., 2006). Repositioning and neurite remodeling observed at 5 and 7 dpi are likely prerequisites for functional integration and survival, as most horizontal cells failing to reposition appear to die. Indeed, approximately half of the analyzed cells successfully repositioned, similar to the survival rate from bromodeoxyuridine (BrdU) labeling analyses (Ge et al., 2006). Hippocampus-engaged EE enhanced repositioning of newborn DGCs, and the increase in neurite branches in animals exposed to EE, is consistent with recent studies showing that hippocampal-engaging experience increases neurite growth in these cells during synapse integration (Gonçalves et al., 2016).

Genes associated with metabolism are activated during the proliferation and differentiation of NSCs (Gonçalves et al., 2016). Therefore, the generation and integration of new DGCs—which include dynamic neurite genesis, neuronal migration, and circuit formation—likely entail high metabolic demands. Recent metabolomics analyses revealed there is an accumulation of sphingolipids in early brain development (Olsen and Færgeman, 2017). Here, we observed an upregulation of sphingolipid-related gene expression, particularly S1PR1, in newly generated DGCs, which was necessary and sufficient for neurite arborization and horizontal-to-radial repositioning of these cells. Although based on our lipidomics data, we observed significant lipid profile differences between the neurogenic region of the DG and the non-neurogenic region of the neocortex, one limitation of this finding is that it represents a single snapshot in time. Lastly, the S1PR1 pathway largely accounted for activity-induced cellular repositioning of new DGCs. However, S1PR1 expression decreases during DGC development (Figure S1), and whether S1PR1 regulates mature DGC activity remains to be determined. We investigated whether forced overexpression of S1PR1 at the earliest developmental stage (e.g., 3 dpi) could facilitate the horizontal-to-radial transition but found that early S1PR1 overexpression influences cell fate determination (data not shown). Related to the timing of expression of S1PR1, we found that expression of S1PR1 is largely turned down after 7 dpi (Figure S1); however, at this time point, cells with lower S1PR1 expression are more likely to be radially oriented, and thus S1PR1 levels may also serve as a functional cellular biomarker predicting which cells are likely to successfully integrate in subsequent days to weeks (Figure S2).

The low levels of S1P we observed in the DG (Figure 2) were surprising. Perhaps S1P that is generated is rapidly bound to the receptor, internalized, and metabolized by S1P lyase, or it is recycled to sphingosine via cytoplasmic S1P phosphatase (Le Stunff et al., 2004). As activated S1PR1 is normally rapidly internalized or trafficked, it is plausible that an increased expression of its level leads to increased S1P degradation and a consequent facilitation of the horizontal-to-radial repositioning.

One limitation of our knockdown approach is that we cannot entirely exclude the possibility that the effects of S1PR1 knockdown on repositioning (Figure 3) could have been partially accounted for by off-target effects on infected neighboring neurons. This possibility is unlikely, however, given the low-titer shS1PR1 used for knockdown experiments; thus, neighboring cells were rarely targeted together. We also observed significantly lower levels of S1PR1 in radial versus horizontal WT DGCs of the same age (Figure S2), supporting our hypothesis. Finally, this study leaves unresolved the potential influence of other S1P receptors expressed in the adult DG (S1PR2–S1PR4) on DGC development.

The discovery of S1P signaling as an essential component of DGC development leads to new questions regarding how this signaling pathway governs the process of circuit integration and what other roles it may play in the developing and adult brain. This signaling pathway is not exclusive to the hippocampus in the adult brain. For example, we recently reported that S1P, as well as its metabolites, are present throughout the adult brain, including the cerebellum, where loss of intrinsic S1P homeostasis induces Purkinje cell degeneration and ataxia (Wang et al., 2015). Future studies will clarify the range of actions by which the S1P signaling pathway affects neuronal development and physiology.

STAR★METHODS

LEAD CONTACT AND MATERIALS AVAILABILITY

Further information and requests for resources and reagents should be directed to and will be fulfilled by the Lead Contact, Dr. Shaoyu Ge (shaoyu.ge@stonybrook.edu).

Viruses generated for this study (see Key Resources Table) have been archived in Dr. Ge's laboratory and are available upon request with no restrictions.

EXPERIMENTAL MODEL AND SUBJECT DETAILS

Animal experiments—All surgeries and experimental procedures were approved by the Stony Brook University Animal Use Committee and were in accordance with the guidelines of the National Institutes of Health. Experiments were conducted using 6–8-week-old C57BL/6 mice of both sexes (Charles River Laboratories, Wilmington, MA). For all surgeries, mice were anesthetized with a ketamine/xylazine cocktail (200 mg/kg body weight, intraperitoneal [i.p.]) and administered buprenorphine HCl (0.05 mg/kg, i.p.) for immediate postsurgical analgesia. Mice were placed on a 37°C heating pad immediately after surgery for 2 h to recover. For EE, 4 to 6 novel objects were placed in the animals' cages, if not specified in the text, for 2 days beginning 4 days after retroviral infection, as previously described (Kirschen et al., 2017). For phospho-S1PR1 staining experiments, the animals were housed in home cages and the EE group was then exposed to an EE containing

6 novel objects for 1 hour while the control group was exposed to a fresh home cage for 1 hour. Both groups were sacrificed at 90 minutes.

METHOD DETAILS

Viruses and infection—Retroviral and lentiviral production was performed as previously described (Gu et al., 2012; Wang et al., 2019). High titer viruses were infused (0.5 μL/injection site) into the dentate gyrus at two sites (stereotaxic coordinates: 2.0 mm from bregma, ± 1.6 mm lateral, 2.5 mm dorsoventral; −3.0 mm from bregma, ± 2.6 mm lateral, 3.2 mm dorsoventral) as described previously (Ge et al., 2006; van Praag et al., 2002). For S1PR1 overexpression, lenti-*GFAP-Cre* was co-infused with pUX-*DF-S1PR1* in order to deliver *Cre recombinase and double floxed S1PR1* into active NPCs, similar to what we previously described (Wang et al., 2019). Expression of shRNAs in the knockdown experiments was induced at 3 dpi and overexpression of S1PR1 was induced at 4 dpi by adding 5 mM doxycycline (2 mg/mL in a 0.4 M sucrose solution) to the animals' drinking water (Kumamoto et al., 2012; Rao et al., 2018).

Slice physiology and imaging—Electrophysiological recordings were obtained at 32°C – 34°C. Labeled newborn DGCs were identified by their fluorescence, location within the subgranular zone or granule cell layer. We monitored the resting membrane potential using the Axopatch 200B instrument right after the establishment of whole cell recording mode. Microelectrodes (4–6 M) were filled in general if not specified in the text with the following (in mM): 120.0 potassium gluconate, 15 KCl, 4 MgCl2, 0.1 EGTA, 10.0 HEPES, 4 MgATP, 0.3 Na3GTP, 7 phosphocreatine (pH 7.4, 300 mOsm). Additional drugs were used with the following final concentrations in the bath: bicuculline (5 μM), TTX (1 μM), CNQX (50 μM) and AP5 (50 μM). Data were collected via a DigiData 1322A (Axon Instruments) at 10 kHz. The series and input resistances were monitored and only those with changes less than 20% during experiments were analyzed. The series resistance ranged between 10–30 ohm and was uncompensated. For stimulation, a bipolar electrode (World Precision Instruments) was used to stimulate (100 μs duration) the perforant pathway input to the dentate gyrus for evoked glutamatergic transmission, and granule cell layer for GABAergic synaptic transmission. The stimulus intensity (~30 μA) were maintained for all experiments. To examine the evoked synaptic transmission, a train of 20 stimuli were delivered at 0.1 Hz. To confirm a lack of evoked synaptic transmission, the stimulation intensity was then increased to 200 μA.

For live imaging, mice received injections of a GFP retrovirus as described above in the section Viruses and infection and were then perfused with chilled (4 °C) slice culture medium (50% Eagle's Base 1 essential medium, 25% Eagle's balanced salt solution, 25% horse serum, 25 mM HEPES-Na, 0.5 mM l-glutamate, 25 mM glucose, 100 × penicillin/streptomycin) at 4 dpi, as previously described (Kleine Borgmann et al., 2013). The brains were extracted and sectioned into 100-mm coronal sections and placed in a CV1000 (Olympus) incubator at 37°C with 5% CO_2 for imaging with a spinning disc confocal microscope at 30-min intervals with a high-throughput live imaging system. A 20× objective was used and imaged a 200×200 μm field of view.

Tissue processing, imaging, and quantification—Mice were deeply anesthetized with urethane (200 mg/kg) and perfused transcardially with phosphate-buffered saline followed by 4% formaldehyde. The brains were removed, fixed overnight in 4% formaldehyde, transferred to a 30% (wt/vol) sucrose solution, and stored at 4°C. The brains were sectioned into 80-mm coronal sections to avoid disrupting cell clusters, covering the entire anterior/posterior axis of the DG. Immunohistochemistry was performed by blocking sections in 1% donkey serum in phosphate-buffered saline with 0.025% Triton for 1 h at room temperature and then incubating them overnight with shaking at 4°C with the following primary antibodies: GFP (rabbit polyclonal antibody, 1:1,000; Sigma-Aldrich, St. Louis, MO), Prox1 (mouse monoclonal, 1:500; Millipore, Burlington, MA), DCX (goat polyclonal antibody, 1:1,000; Santa Cruz Biotechnology, Dallas, TX), S1PR1 (rabbit polyclonal antibody, 1:500; Abcam, Cambridge, UK), phospho-S1PR1 (rabbit polyclonal antibody, 1:500, Abcam, Cambridge, UK- requires antigen retrieval protocol as previously described (Rao et al., 2018)). The sections were then incubated for 3 h with shaking at room temperature with the following secondary antibodies: Alexa 488-conjugated donkey anti-rabbit antibody (1:1,000; The Jackson Laboratory, Bar Harbor, ME), and Alexa 594-conjugated donkey anti-goat (1:1,000; Abcam).

Images were obtained on an Olympus FV1000 confocal microscope. The neurite morphology of the newly generated DGCs was determined in Imaris or ImageJ. The angle of the cellular axis with respect to a line parallel to the granule cell layer was measured using the angle tool in ImageJ. Confocal images of dendritic trees were analyzed in ImageJ using the Neuron J plugin.

RNA-seq analysis of *in vitro* differentiated neurons—The neuronal stem cell (NSCs) cultures were derived from hippocampal neural stem cells based on previously published protocols. To induce neuronal differentiation, we treated hippocampal neural stem cells with retinoic acid (1 μM) and forskolin (5 μM) as previously described in a study in which neuronal differentiation was characterized by upregulation of Neurod1 and downregulation of Sox2 by western blotting in NSCs and neuronal cultures (Gao et al., 2011; Kuwabara et al., 2009). Twenty-four hours after differentiation, RNA was isolated and RNA-seq was performed as previously described (Mukherjee et al., 2016). Two replicates of differentiated neurons and four replicates of proliferating neural stem cells were used for RNA-sequencing and data analysis. Differential gene expression analysis was performed using R package DESeq2 (Love et al., 2014).

Lipidomics—Animals were first transcardially perfused with PBS to clear blood from the system. Their brains were collected, acutely dissected, flash frozen in a dry ice ethanol bath, and stored at −80°C. Protein levels were measured via bicinchoninic acid assay to normalize samples to total protein content. Samples were then submitted to the Lipidomics Core at Stony Brook University for lipid species quantification by high-performance liquid chromatography and mass spectrometry, as previously described (Bielawski et al., 2006).

QUANTIFICATION AND STATISTICAL ANALYSIS

Data were analyzed with independent-samples Student's t tests, one-way and two-way analyses of variance (ANOVAs) followed by least significant difference tests, one-way ANOVAs with repeated-measures followed by the Pearson correlation analysis, Mann-Whitney *U* test and the Kruskal-Wallis test. Two-tailed *P* values of < 0.05 were considered the cutoff for statistical significance. All data are represented as the mean ± standard errors. Samples sizes (*n*) represent the numbers of animals unless otherwise specified.

DATA AND CODE AVAILABILITY

This study did not generate any original code or databases. Original datasets are available on request (lead contact: Dr. Shaoyu Ge, shaoyu.ge@stonybrook.edu).

Supplementary Material

Refer to Web version on PubMed Central for supplementary material.

ACKNOWLEDGMENTS

We thank Dr. Simon Halegoua for critical feedback on this manuscript and Dr. Maya Shelly for technical support of *in vitro* cell analysis. We also thank the members of Dr. S. Ge's and Dr. Q. Xiong's laboratories for valuable comments. This work was supported by the NIH (grants AG046875 and NS104868 to S.G., NS093992 to J.H., and NS089770 to S.G. and J.H.) and partially by the SUNY Brain Excellence. C.-H.Y. is under the support of MOST-103 (106)-2320-B038–027-MY3. This work was also partially supported by funds from the Semmes Foundation, Inc. and the Robert J. Kleberg, Jr. and Helen C. Kleberg Foundation (to J.H.).

REFERENCES

Altman J, and Das GD (1965). Autoradiographic and histological evidence of postnatal hippocampal neurogenesis in rats. J. Comp. Neurol. 124, 319–335. [PubMed: 5861717]

Bielawski J, Szulc ZM, Hannun YA, and Bielawska A (2006). Simultaneous quantitative analysis of bioactive sphingolipids by high-performance liquid chromatography-tandem mass spectrometry. Methods 39, 82–91. [PubMed: 16828308]

Chavez A, Schmidt TT, Yazbeck P, Rajput C, Desai B, Sukriti S, Giantsos-Adams K, Knezevic N, Malik AB, and Mehta D (2015). S1PR1 Tyr143 phosphorylation downregulates endothelial cell surface S1PR1 expression and responsiveness. J. Cell Sci. 128, 878–887. [PubMed: 25588843]

Christian KM, Song H, and Ming GL (2014). Functions and dysfunctions of adult hippocampal neurogenesis. Annu. Rev. Neurosci. 37, 243–262. [PubMed: 24905596]

Eriksson PS, Perfilieva E, Björk-Eriksson T, Alborn AM, Nordborg C, Peterson DA, and Gage FH (1998). Neurogenesis in the adult human hippocampus. Nat. Med. 4, 1313–1317. [PubMed: 9809557]

Espósito MS, Piatti VC, Laplagne DA, Morgenstern NA, Ferrari CC, Pitossi FJ, and Schinder AF (2005). Neuronal differentiation in the adult hippocampus recapitulates embryonic development. J. Neurosci. 25, 10074–10086. [PubMed: 16267214]

Gao Z, Ure K, Ding P, Nashaat M, Yuan L, Ma J, Hammer RE, and Hsieh J (2011). The master negative regulator REST/NRSF controls adult neurogenesis by restraining the neurogenic program in quiescent stem cells. J. Neurosci. 31, 9772–9786. [PubMed: 21715642]

Ge S, Goh EL, Sailor KA, Kitabatake Y, Ming GL, and Song H (2006). GABA regulates synaptic integration of newly generated neurons in the adult brain. Nature 439, 589–593. [PubMed: 16341203]

Gonçalves JT, Schafer ST, and Gage FH (2016). Adult Neurogenesis in the Hippocampus: From Stem Cells to Behavior. Cell 167, 897–914. [PubMed: 27814520]

Gu Y, Arruda-Carvalho M, Wang J, Janoschka SR, Josselyn SA, Frankland PW, and Ge S (2012). Optical controlling reveals time-dependent roles for adult-born dentate granule cells. Nat. Neurosci. 15, 1700–1706. [PubMed: 23143513]

Hannun YA, and Obeid LM (2008). Principles of bioactive lipid signalling: lessons from sphingolipids. Nat. Rev. Mol. Cell Biol. 9, 139–150. [PubMed: 18216770]

He S, Li Z, Ge S, Yu YC, and Shi SH (2015). Inside-Out Radial Migration Facilitates Lineage-Dependent Neocortical Microcircuit Assembly. Neuron 86, 1159–1166. [PubMed: 26050035]

Kempermann G, Kuhn HG, and Gage FH (1997). More hippocampal neurons in adult mice living in an enriched environment. Nature 386, 493–495. [PubMed: 9087407]

Kirschen GW, Shen J, Tian M, Schroeder B, Wang J, Man G, Wu S, and Ge S (2017). Active Dentate Granule Cells Encode Experience to Promote the Addition of Adult-Born Hippocampal Neurons. J. Neurosci. 37, 4661–4678. [PubMed: 28373391]

Kleine Borgmann FB, Bracko O, and Jessberger S (2013). Imaging neurite development of adult-born granule cells. Development 140, 2823–2827. [PubMed: 23720045]

Kumamoto N, Gu Y, Wang J, Janoschka S, Takemaru K, Levine J, and Ge S (2012). A role for primary cilia in glutamatergic synaptic integration of adult-born neurons. Nat. Neurosci. 15, 399–405, S1. [PubMed: 22306608]

Kuwabara T, Hsieh J, Muotri A, Yeo G, Warashina M, Lie DC, Moore L, Nakashima K, Asashima M, and Gage FH (2009). Wnt-mediated activation of NeuroD1 and retro-elements during adult neurogenesis. Nat. Neurosci. 12, 1097–1105. [PubMed: 19701198]

Le Stunff H, Milstien S, and Spiegel S (2004). Generation and metabolism of bioactive sphingosine-1-phosphate. J. Cell. Biochem. 92, 882–899. [PubMed: 15258913]

Lee MJ, Thangada S, Paik JH, Sapkota GP, Ancellin N, Chae SS, Wu M, Morales-Ruiz M, Sessa WC, Alessi DR, and Hla T (2001). Akt-mediated phosphorylation of the G protein-coupled receptor EDG-1 is required for endothelial cell chemotaxis. Mol. Cell 8, 693–704. [PubMed: 11583630]

Love MI, Huber W, and Anders S (2014). Moderated estimation of fold change and dispersion for RNA-seq data with DESeq2. Genome Biol. 15, 550. [PubMed: 25516281]

Mukherjee S, Brulet R, Zhang L, and Hsieh J (2016). REST regulation of gene networks in adult neural stem cells. Nat. Commun. 7, 13360. [PubMed: 27819263]

Olsen ASB, and Færgeman NJ (2017). Sphingolipids: membrane microdomains in brain development, function and neurological diseases. Open Biol. 7, 170069.

Overstreet Wadiche L, Bromberg DA, Bensen AL, and Westbrook GL (2005). GABAergic signaling to newborn neurons in dentate gyrus. J. Neurophysiol. 94, 4528–4532. [PubMed: 16033936]

Overstreet-Wadiche LS, Bromberg DA, Bensen AL, and Westbrook GL (2006). Seizures accelerate functional integration of adult-generated granule cells. J. Neurosci. 26, 4095–4103. [PubMed: 16611826]

Rao S, Kirschen GW, Szczurkowska J, Di Antonio A, Wang J, Ge S, and Shelly M (2018). Repositioning of Somatic Golgi Apparatus Is Essential for the Dendritic Establishment of Adult-Born Hippocampal Neurons. J. Neurosci. 38, 631–647. [PubMed: 29217690]

Sahay A, Scobie KN, Hill AS, O'Carroll CM, Kheirbek MA, Burghardt NS, Fenton AA, Dranovsky A, and Hen R (2011). Increasing adult hippocampal neurogenesis is sufficient to improve pattern separation. Nature 472, 466–470. [PubMed: 21460835]

Scharfman H, Goodman J, and McCloskey D (2007). Ectopic granule cells of the rat dentate gyrus. Dev. Neurosci. 29, 14–27. [PubMed: 17148946]

Song J, Sun J, Moss J, Wen Z, Sun GJ, Hsu D, Zhong C, Davoudi H, Christian KM, Toni N, et al. (2013). Parvalbumin interneurons mediate neuronal circuitry-neurogenesis coupling in the adult hippocampus. Nat. Neurosci. 16, 1728–1730. [PubMed: 24212671]

Sun GJ, Zhou Y, Stadel RP, Moss J, Yong JH, Ito S, Kawasaki NK, Phan AT, Oh JH, Modak N, et al. (2015). Tangential migration of neuronal precursors of glutamatergic neurons in the adult mammalian brain. Proc. Natl. Acad. Sci. USA 112, 9484–9489. [PubMed: 26170290]

Tashiro A, Sandler VM, Toni N, Zhao C, and Gage FH (2006). NMDA-receptor-mediated, cell-specific integration of new neurons in adult dentate gyrus. Nature 442, 929–933. [PubMed: 16906136]

van Praag H, Schinder AF, Christie BR, Toni N, Palmer TD, and Gage FH (2002). Functional neurogenesis in the adult hippocampus. Nature 415, 1030–1034. [PubMed: 11875571]

Wang K, Xu R, Schrandt J, Shah P, Gong YZ, Preston C, Wang L, Yi JK, Lin CL, Sun W, et al. (2015). Alkaline Ceramidase 3 Deficiency Results in Purkinje Cell Degeneration and Cerebellar Ataxia Due to Dyshomeostasis of Sphingolipids in the Brain. PLoS Genet. 11, e1005591.

Wang J, Shen J, Kirschen GW, Gu Y, Jessberger S, and Ge S (2019). Lateral dispersion is required for circuit integration of newly generated dentate granule cells. Nat. Commun. 10, 3324. [PubMed: 31346164]

Highlights

- Dentate granule cells undergo repositioning before circuit integration
- Sphingolipid signaling is promptly activated and regulates repositioning
- S1PR1 is activated by hippocampus-engaged behavior and regulates the repositioning

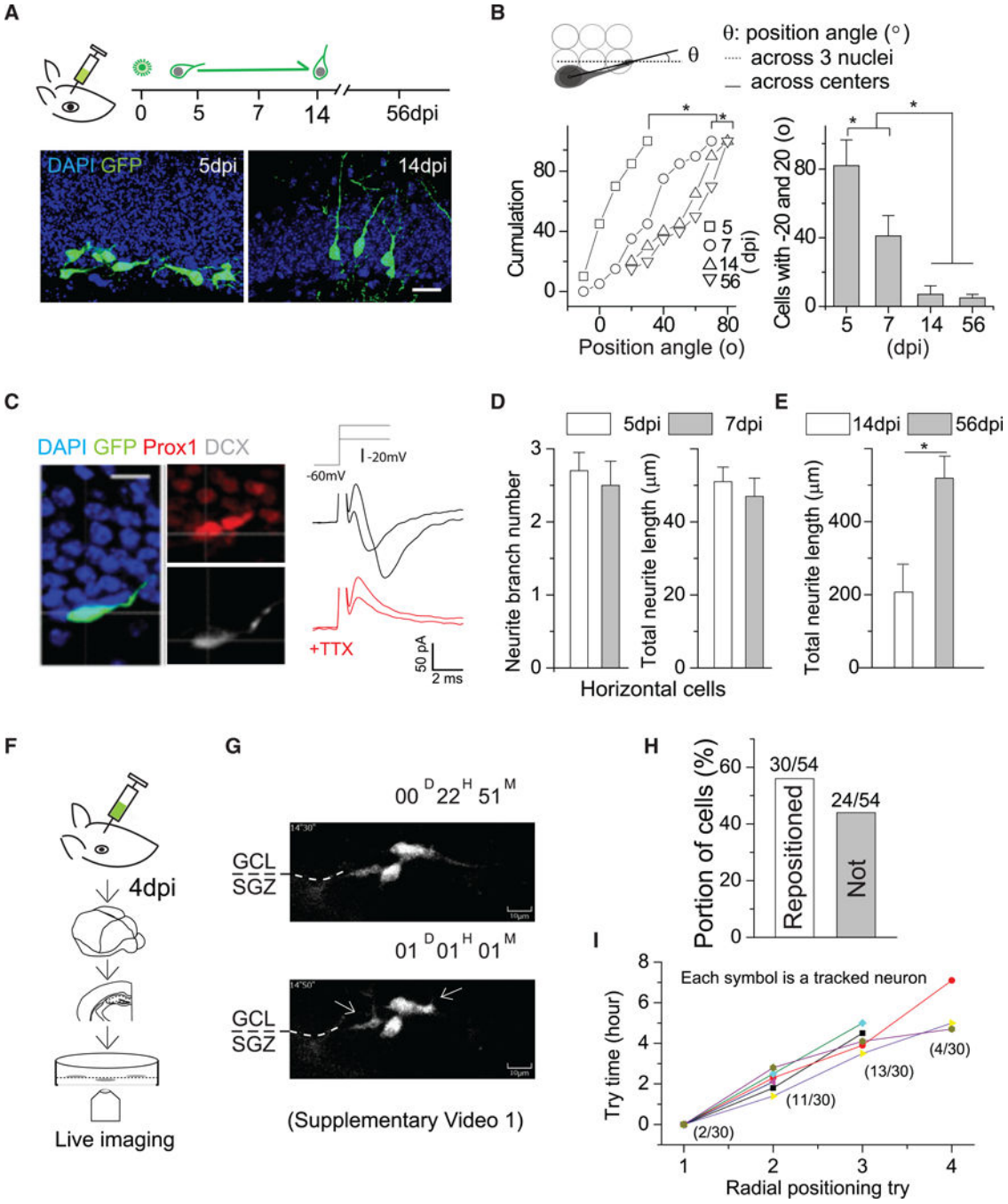

Figure 1. Newly Generated DGCs Undergo Horizontal-to-Radial Repositioning via Neurite Remodeling

(A) (Top) Schematic showing the procedure and timeline for retroviral labeling of newly generated DGCs in adult mice. (Bottom) Representative images of new DGCs at 5 and 14 dpi. Scale bar, 20 μm.

(B) (Top) Schematic showing the strategy for angle measurement. (Bottom) Summary plot of angle distributions of newly generated DGCs at 5, 7, 14, and 56 dpi. 5 dpi, 37 cells from 4 mice; 7 dpi, 59 cells from 5 mice; 14 dpi, 31 cells from 3 mice; 56 dpi, 26 cells from 3 mice.

Komolgorov-Smirnov test, *p < 0.05, left. One-way ANOVA followed by post hoc LSD tests, *p < 0.05, right.

(C) (Left) DCX and Prox1 immunostaining of horizontal new DGCs at 5 dpi. (Right) Sample recording traces of Na^+ currents from horizontal GFP^+ cells at 5 dpi. Scale bar, 10 μm.

(D) Summary plots of the numbers (left) and lengths (right) of neurites from new DGCs at 5 and 7 dpi. Both groups were not statistically significant. Student's t test(n = 3–4 mice).

(E) Plot of total neurite length of DGCs at 14 and 56 dpi. Student's t test, *p < 0.05 (n = 3–4 mice).

(F) Illustration showing the experimental slice culture procedure.

(G) Sequential views of two typical newborn DGCs repositioning during the first day of imaging (5 dpi). The full video is presented in Video S1.

(H) Summary plot showing the proportion of analyzed cells that have either succeeded or failed in repositioning.

(I) Summary plot for the attempts of cells to transit and succeeded in repositioning. From attempt to attempt, the interval is ~2 h. The parentheses indicate the proportion of cells that made the transition during that attempt to do so. Error bars represent standard error of mean.

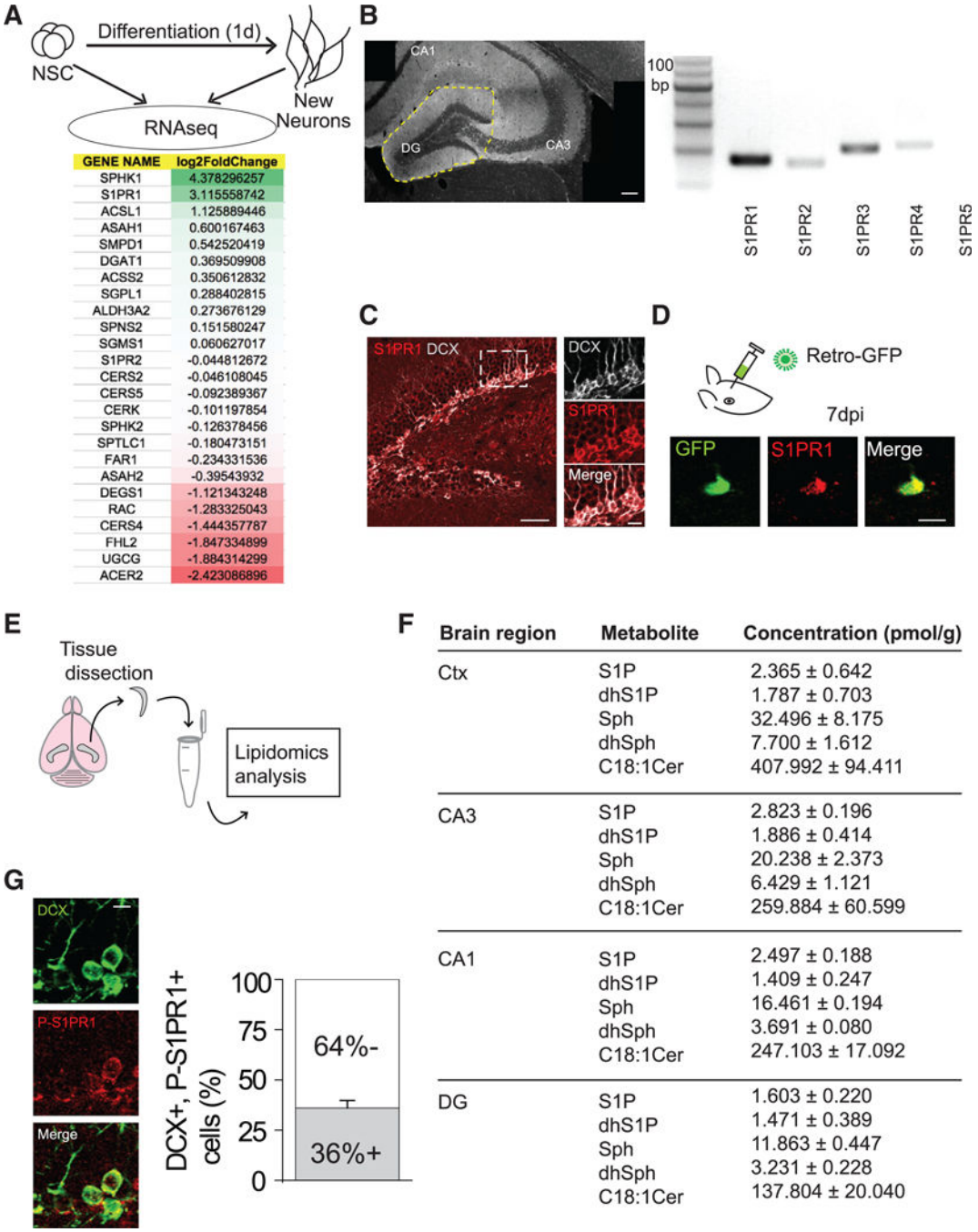

GENE NAME	log2FoldChange
SPHK1	4.378296257
S1PR1	3.115558742
ACSL1	1.125889446
ASAH1	0.600167463
SMPD1	0.542520419
DGAT1	0.369509908
ACSS2	0.350612832
SGPL1	0.288402815
ALDH3A2	0.273676129
SPNS2	0.151580247
SGMS1	0.060627017
S1PR2	-0.044812672
CERS2	-0.046108045
CERS5	-0.092389367
CERK	-0.101197854
SPHK2	-0.126378456
SPTLC1	-0.180473151
FAR1	-0.234331536
ASAH2	-0.39543932
DEGS1	-1.121343248
RAC	-1.283325043
CERS4	-1.444357787
FHL2	-1.847334899
UGCG	-1.884314299
ACER2	-2.423086896

Brain region	Metabolite	Concentration (pmol/g)
Ctx	S1P	2.365 ± 0.642
	dhS1P	1.787 ± 0.703
	Sph	32.496 ± 8.175
	dhSph	7.700 ± 1.612
	C18:1Cer	407.992 ± 94.411
CA3	S1P	2.823 ± 0.196
	dhS1P	1.886 ± 0.414
	Sph	20.238 ± 2.373
	dhSph	6.429 ± 1.121
	C18:1Cer	259.884 ± 60.599
CA1	S1P	2.497 ± 0.188
	dhS1P	1.409 ± 0.247
	Sph	16.461 ± 0.194
	dhSph	3.691 ± 0.080
	C18:1Cer	247.103 ± 17.092
DG	S1P	1.603 ± 0.220
	dhS1P	1.471 ± 0.389
	Sph	11.863 ± 0.447
	dhSph	3.231 ± 0.228
	C18:1Cer	137.804 ± 20.040

Figure 2. Newly Generated DGCs Highly Express S1PR1

(A) (Top) Procedure for RNA-seq analysis of new neurons 1 day after differentiating from adult hippocampal neural stem cells. (Bottom) Expression profiling of sphingolipid signaling-related genes. Mann-Whitney U test, SPHK1 p = 0.064, S1PR1 p = 0.064, ACSL1 p = 0.064, ASAH1 p = 0.064, SMPD1 p = 0.064, DGAT1 p = 0.064, ACSS2 p = 0.355, SGPL1 p = 0.064, ALDH3A2 p = 0.04, SPNS2 p = 1.000, SGMS1 p = 0.064, S1PR2 p = 0.165, CERS2 p = 0.064, CERS5 p = 0.355, CERK p = 0.355, SPHK2 p = 0.064, SPTLC1 p

= 1.000, FAR1 p = 0.064, ASAH2 p = 0.643, DEGS1 p = 0.060, RAC p = 0.165, CERS4 p = 0.064, FHL2 p =1.000, UGCG p = 0.06, ACER2 p = 0.643.

(B) (Left) Region of dentate gyrus dissected. (Right) S1PR isoform mRNA detection (S1PR5 was not detected). Scale bar, 100 μm.

(C) (Left) Representative image of the dentate gyrus immunostained for DCX and S1PR1. Scale bar, 50 μm. (Right) Magnified view of the region outlined in the image on the left. Scale bar, 10 μm. (Related to Figures S1 and S2).

(D) (Top) Retroviral GFP was delivered to the DG to label newly born DGCs. (Bottom) Representative image showing expression of S1PR1 in a DGC at 7 dpi. Scale bar, 10 μm.

(E) Schematic of hippocampal/cortical dissection and lipidomics analysis.

(F) Concentrations of various sphingolipid metabolites in several brain regions. DG versus Ctx: $p < 0.0001$ (two-way ANOVA), followed by post hoc LSD tests, Sph $p < 0.05$, dhSph $p < 0.05$, S1P $p = 0.32$, dsS1P $p = 0.738$, Cer18:1 $p < 0.001$. Experiment repeated in triplicates. Cer, ceramide; Ctx, cortex; DG, dentate gyrus; S1P, sphingosine1-phosphate; dhS1P, dihydrosphingosine 1phosphate; Sph, sphingosine; dhSph, dihydrosphingosine.

(G) (Left) Representative image of DCX and phospho (Thr236)-S1PR1 (P-S1PR1) immunostaining in the DG. Scale bar, 10 μm. (Right). Quantification of the proportion of DCX^+ cells immunopositive for P-S1PR1 (n = 3–4). Error bars represent standard error of mean.

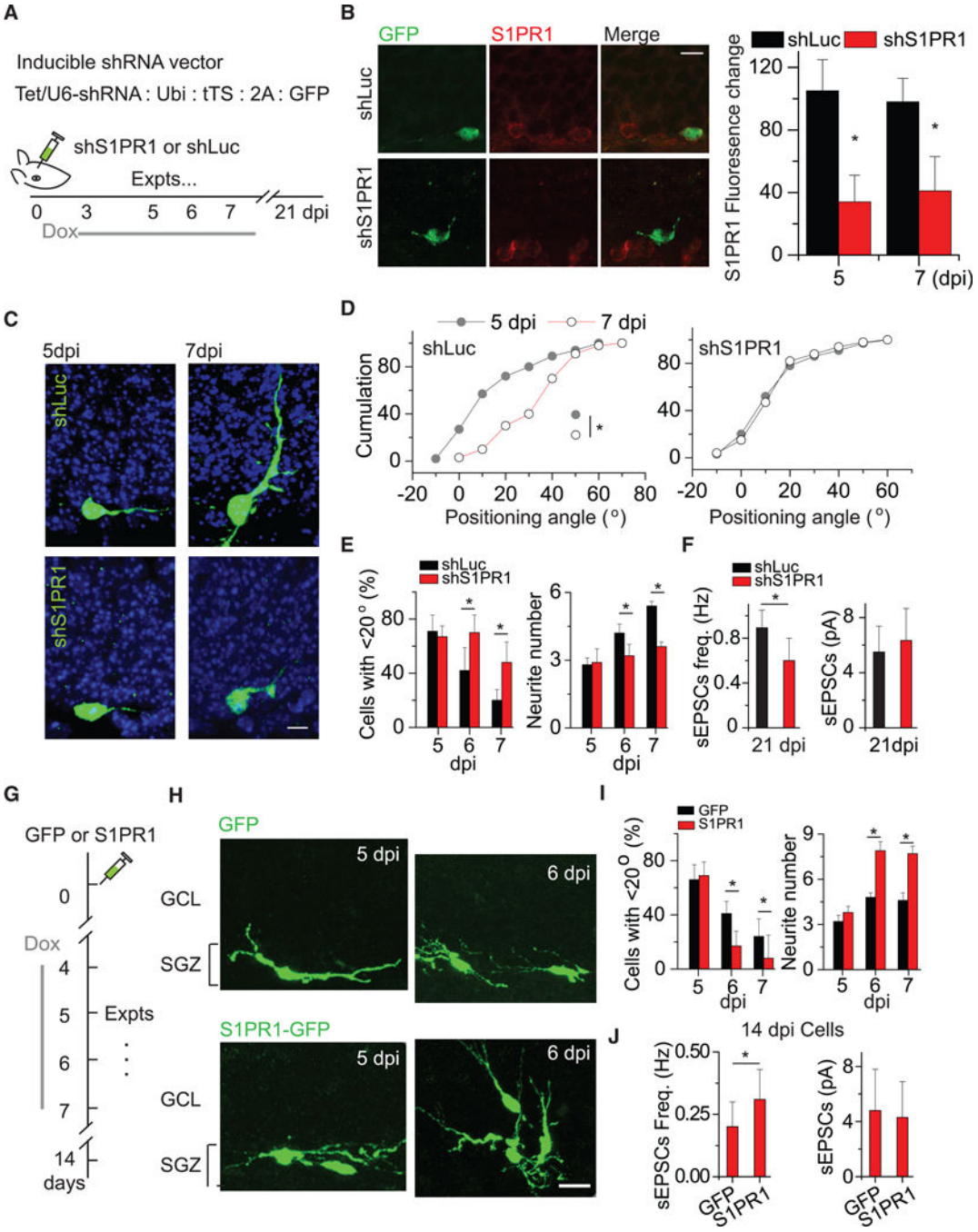

Figure 3. S1PR1 Knockdown Reduces Neurite Growth and Horizontal-to-Radial Repositioning

(A) Description of shRNA expression vector and experimental timeline of shRNA viral injection and doxycycline induction.

(B) (Left) Representative images of S1PR1 expression in shS1PR1^{+} and shLuc^{+} DGCs at 5 dpi. (Right) Summary plot of the S1PR1 fluorescent signal intensity. *$p < 0.05$ (two-tailed unpaired t test).

(C) Representative images of shS1PR1^{+} and shLuc^{+} newborn DGCs and their morphological maturation at 5 and 7 dpi.

(D) Cumulative distribution plots of positioning angles of shS1PR1$^+$ and shLuc$^+$ DGCs at 5 and 7 dpi. *$p < 0.05$ ($n = 5$ for shLuc group and $n = 7$ for shS1PR1; Kolmogorov-Smirnov tests).

(E) Summary of the proportions of cells with an angle <20°at 5, 6, and 7 dpi. *$p < 0.05$ ($n = 5$ for shLuc group and $n = 7$ for shS1PR1; two-way ANOVA followed by post hoc LSD tests).

(F) Glutamatergic synaptic transmission recorded from shLuc and shS1PR1 adult-born DGCs at 21 dpi ($n = 6$ neurons from 3 mice for each, unpaired t tests, *$p < 0.05$).

(G) Schematic for examining the effect of S1PR1 expression on the repositioning of newly generated DGCs.

(H) Representative images of new DGCs with GFP only or S1PR1 expression. Scale bar, 15 μm.

(I) Plot of the numbers of position angles and neurite branches of control and shRNA-expressing cells at 5, 6, and 7 dpi. The statistics are the same as described for (E) ($n = 3$ for GFP and $n = 6$ for S1PR1-GFP).

(J) Glutamatergic synaptic transmission recorded from GFP and GFP-S1PR1 newly generated DGCs at 14 dpi ($n = 7$ neurons from 3–4 mice, *$p < 0.05$). Expts, experiments. Error bars represent standard error of mean.

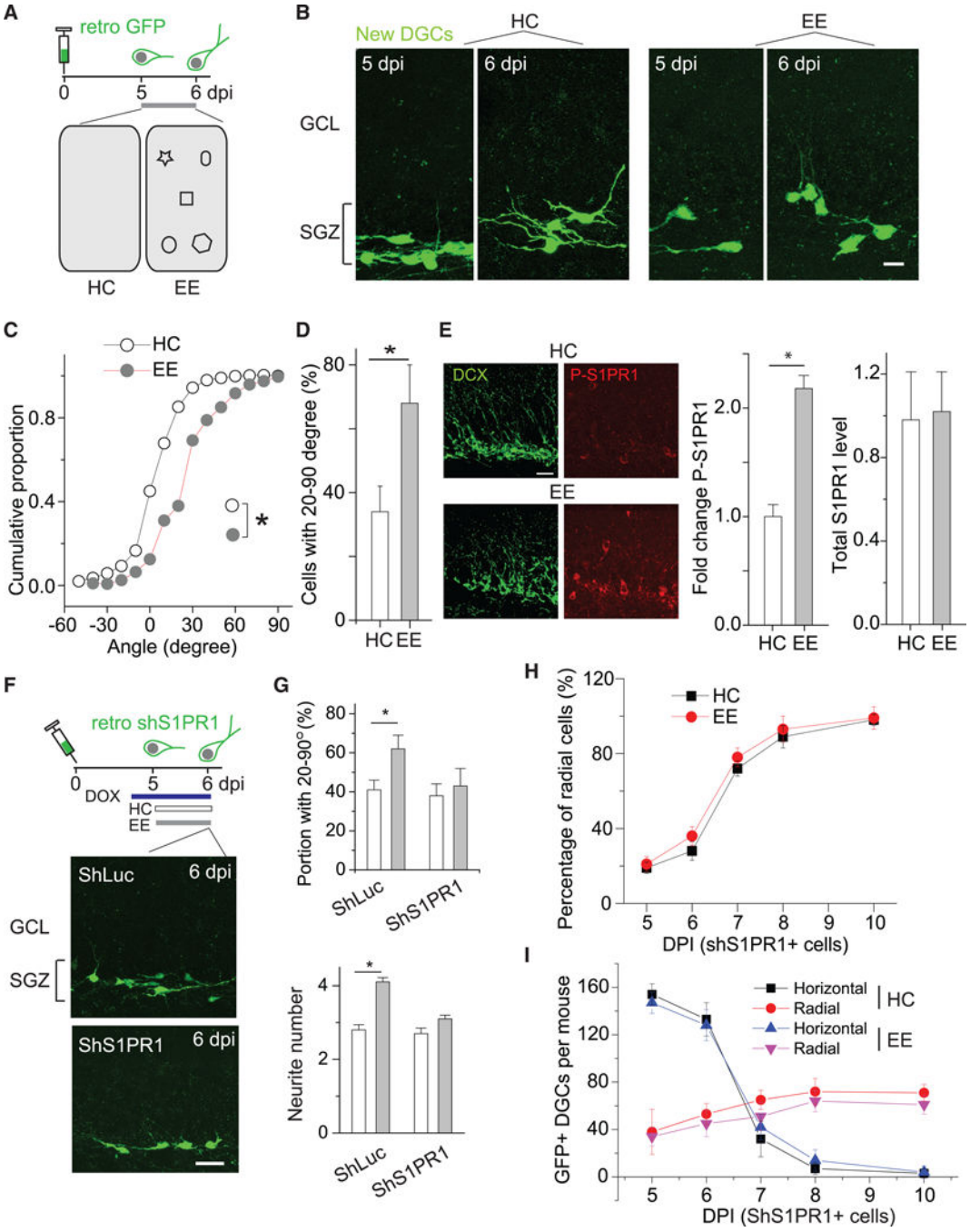

Figure 4. Environmental Enrichment Accelerates the Horizontal-to-Radial Repositioning of Newly Generated DGCs via S1PR1 Activation

(A) Schematic showing the experimental design, including the timeline for viral labeling and experiments (top) and two environments, HC and EE (bottom). HC, home cage; EE, enriched environment.

(B) Sample images of GFP$^+$ newly generated DGCs at 5 and 6 dpi from both HC and EE conditions. Scale bar, 10 μm.

(C) Plot of the distribution of primary neurite angles of newly generated DGCs under either HC or EE conditions. *p < 0.05 (n = 5 mice for HC and n = 6 for EE; Kolmogorov-Smirnov test).

(D) Summary plot of the proportion of newly generated DGCs with radial primary neurites of 20°−90°at 6 dpi under HC and EE conditions. *p < 0.05 (n = 3–4 mice; two-tailed unpaired t test).

(E) (Left) Representative images showing phosph-S1PR1 in DCX^+ new DGCs under HC and EE conditions. (Right) Summary of S1PR1 and P-S1PR1 levels in DCX^+ cells. *p < 0.05 (n = 4 mice for HC and n = 3 for EE; two-tailed unpaired t tests).

(F) Experimental outline (top) and representative images of GFP^+ shS1PR1- and shLuc-expressing DGCs at 6 dpi (bottom) under HC conditions. Scale bar, 20 μm.

(G) Summary of the portion of DGCs with angles between 20°and 90°at 6 dpi from mice under HC and EE conditions. *p < 0.05 (shLuc), p = 0.330 (shS1PR1) (two-tailed unpaired t test) (top). Summary of the numbers of neurites from DGCs at 6 dpi from mice under HC and EE conditions. *p < 0.01 (shLuc), p > 0.05 (shS1PR1) (n = 5 mice; two-tailed unpaired t test) (bottom). Related to Figures S3 and S4.

(H) Summary of percentages of radially positioned GFP^+ DGCs at 5, 6,7,8,and10 dpi under HC and EE conditions(n= 3–5mice per group and developmental stage).

(I) Summary of the numbers of GFP^+ DGCs (shS1PR1) at 5, 6, 7, 8, and 10 dpi under HC and EE conditions (n = 3–5 mice per group and developmental stage). Error bars represent standard error of mean.

KEY RESOURCES TABLE

REAGENT or RESOURCE	SOURCE	IDENTIFIER
Antibodies		
rabbit polyclonal anti-GFP	Sigma-Aldrich	Cat# SAB4301138; RRID: AB_2750576
Millipore mouse monoclonal anti-Prox1	Millipore	Cat# MAB5654; RRID: AB_2170714
goat polyclonal anti-DCX	Santa Cruz Biotechnology, Dallas, TX	Sc-8066
rabbit polyclonal anti- S1PR1	Abcam, Cambridge, UK	Cat# ab77076; RRID: AB_1523525
Rabbit polyclonal anti-S1PR1 phospho T236	Abcam, Cambridge, UK	Ab111571
Bacterial and Virus Strains		
pUX-*pTet-Ubi-shLuc*	This manuscript	Available on request
pUX-*pTet-Ubi-shS1PR1-GFP*	This manuscript	Available on request
pUX-*pTet-Ubi-DF-S1PR1-GFP*	This manuscript	Available on request
Lenti-*GFAP-Cre*	This manuscript	Available on request
Chemicals, Peptides, and Recombinant Proteins		
Forskolin	Sigma-Aldrich	66575–29-9
Retinoic acid	Sigma-Aldrich	302–79-4
Experimental Models: Cell Lines		
Hippocampal neural stem cells derived from Wildtype C57BL/6 mice	Charles River Laboratories, Wilmington, MA	C57BL/6 Mouse
Experimental Models: Organisms/Strains		
6–8-week-old male and female wildtype C57BL/6 mice	Charles River Laboratories, Wilmington, MA	C57BL/6 Mouse